

# Gradient-Free Adversarial Purification with Diffusion Models

Xuelong Dai

Dong Wang

Duan Mingxing

Bin Xiao

## Abstract

*Adversarial training and adversarial purification are two effective and practical defense methods to enhance a model’s robustness against adversarial attacks. However, adversarial training necessitates additional training, while adversarial purification suffers from low time efficiency. More critically, current defenses are designed under the perturbation-based adversarial threat model, which is ineffective against the recently proposed unrestricted adversarial attacks. In this paper, we propose an effective and efficient adversarial defense method that counters both perturbation-based and unrestricted adversarial attacks. Our defense is inspired by the observation that adversarial attacks are typically located near the decision boundary and are sensitive to pixel changes. To address this, we introduce adversarial anti-aliasing to mitigate adversarial modifications. Additionally, we propose adversarial super-resolution, which leverages prior knowledge from clean datasets to benignly recover images. These approaches do not require additional training and are computationally efficient without calculating gradients. Extensive experiments against both perturbation-based and unrestricted adversarial attacks demonstrate that our defense method outperforms state-of-the-art adversarial purification methods.*

## 1. Introduction

Deep learning models have demonstrated remarkable performance across various tasks [14, 22, 36]. With the rapid advancement and widespread deployment of these models, their security and robustness are garnering increasing attention.

It is widely recognized that deep learning models are highly vulnerable to adversarial attacks [3, 23]. These attacks are performed by adding imperceptible perturbations to clean images. The perturbed images, known as adversarial examples, can deceive trained deep learning classifiers with high confidence while appearing natural and realistic to human observers. To mitigate adversarial attacks and ensure the stability of deep learning models, adversarial training [13, 23] has been developed. This approach aims to defend against adversarial attacks by training the classifier

with adversarial examples. However, adversarial training tends to perform poorly against unknown attacks.

Recently, with the development of diffusion models [11, 26], adversarial purification [24, 29] has shown promising defense performance by recovering the adversarial examples to clean images. These works adopt the diffusion model’s reverse generation process to gradually remove the Gaussian noise from the forward process and the adversarial perturbations. Nevertheless, these methods require heavy computational resources during the purification, which may not be practical in real-time scenarios.

Diffusion models also facilitate stronger unrestricted adversarial attacks [5, 6, 9]. These unrestricted adversarial examples (UAEs) are generated through the reverse generation process by incorporating adversarial guidance. Unlike traditional perturbation-based adversarial attacks, UAEs exhibit superior attack performance against current defenses due to their distinct threat models. These attacks pose a new threat to the development of deep learning models and urgently need to be addressed. Even worse, existing defenses have merely covered the discussion against UAEs.

In this paper, we propose an effective adversarial defense method that detects both perturbation-based adversarial examples and unrestricted adversarial examples. To achieve the defense objective, we locate and utilize the common characteristic of these two types of attacks that both adversarial examples are generated close to the decision boundary for minimal perturbations, which makes these adversarial examples susceptible to changes in pixels.

Our defense employs zero-shot adversarial purification by extracting the “semantic shape” information from images without the image details, as illustrated in Figure 1. Specifically, we use adversarial anti-aliasing with specialized filters to blur the detailed adversarial modifications in the adversarial examples. Following this, we apply adversarial super-resolution to the anti-aliased adversarial examples, upscaling the blurred images using details from pre-trained clean super-resolution diffusion models. These two methods are time-efficient and do not require any modifications to the original models. To demonstrate the effectiveness of our proposed defense, we further validate its performance by using the upscaled adversarial examples as input for adversarial purification. Experiments on various datasets show that our defense outperforms state-of-the-art



Figure 1. **The proposed adversarial defense pipeline.** We give an adversarial example of “cock” class with AutoAttack  $\ell_{\text{inf}} = 8/255$  on ImageNet dataset. Adversarial anti-aliasing aims to eliminate adversarial perturbations, while adversarial super-resolution seeks to restore benign images from blurred adversarial examples using prior knowledge from the clean dataset.

adversarial defenses in adversarial purification.

Our contributions are summarized as follows:

- We propose a novel adversarial defense capable of countering both perturbation-based adversarial examples and unrestricted adversarial examples, addressing the current gap in effective defenses against unrestricted adversarial attacks.
- We introduce various zero-shot and gradient-free defense strategies that preserve the semantic information of adversarial examples while eliminating adversarial modifications. These strategies include adversarial anti-aliasing for “semantic” extraction and adversarial super-resolution for incorporating benign priors and recovering benign details from adversarial examples.
- We conduct extensive experiments on various datasets against adaptive adversarial attacks. The results demonstrate the effectiveness of our proposed defense method compared to state-of-the-art adversarial defenses. Moreover, anti-aliased and upscaled adversarial examples effectively integrate with existing diffusion-based adversarial purification, validating the usability and scalability of our approach.

## 2. Background

### 2.1. Adversarial Training

Adversarial training (AT) is one of the most practical methods for enhancing a model’s robustness against adversarial attacks. It involves training the model with both benign and adversarial data simultaneously during the training phase. However, robustness against unseen attacks remains a significant challenge that affects the defense performance of traditional adversarial training [23]. To address this, Gowal et al. [13] and Rebuffi et al. [25] have incorporated generated and augmented data to improve generalization by increasing data diversity. In addition to leveraging diverse data, refining the objective formulation of AT

has also proven effective. By considering model weights, a wide range of adversarial training methods [17, 35] have been proposed.

### 2.2. Adversarial Purification

Adversarial purification aims to eliminate adversarial perturbations in adversarial examples without requiring the re-training of deep learning models. These methods leverage the generative capabilities of generative models. Previous works utilizing generative adversarial networks (GANs) [28] and score-based matching models [31, 37] have demonstrated state-of-the-art performance compared to adversarial training. With the advent of diffusion models, Nie et al. [24] discovered that diffusion-based adversarial purification methods outperform previous approaches in recovering clean images. However, finding the optimal generation steps for diffusion-based adversarial purification remains challenging. Additionally, adversarial images can negatively impact the reverse generation process of diffusion models. To address these issues, several works [20, 29, 33] have proposed various solutions to enhance the performance of adversarial purification.

## 3. Preliminary

### 3.1. Threat Model

Adversarial examples conduct attacks by fooling the target model’s classification result. Considering the untargeted attack scenario, the perturbation-based adversarial examples are defined as:

$$A_{\text{AE}} \triangleq \{x_{\text{adv}} = x + \delta | y \neq f(x), x \in D, |\delta| \leq \epsilon\} \quad (1)$$

where  $\delta$  is the adversarial perturbation,  $f(\cdot)$  is the target model,  $D$  is the clean dataset, and  $\epsilon$  is the perturbation norm constraint.

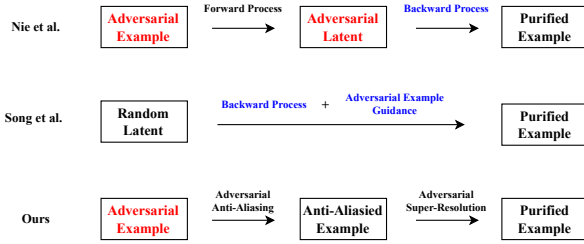


Figure 2. **The comparisons of state-of-the-art diffusion-based adversarial purification pipelines.** We mark the defense process in blue to represent time-consuming approaches. We use red font to indicate non-purified adversarial input.

These adversarial examples are generated by adding the perturbations to the clean images. However, such perturbations can degenerate the image quality. By utilizing the generation models, Song et al. [30] presented unrestricted adversarial examples by directly generating adversarial examples with the generation tasks, which can be formulated as:

$$A_{\text{UAE}} \triangleq \{x_{\text{adv}} \in \mathcal{G}(z_{\text{adv}}, y) | y \neq f(x)\} \quad (2)$$

where  $\mathcal{G}$  is the generation model,  $z_{\text{adv}}$  is the latent code for generation.

These two adversarial examples are generated with different threat models. However, they both can successfully conduct attacks against the given target model. A robust defense method should be able to defend against these attacks simultaneously.

### 3.2. Diffusion-Based Adversarial Purification

The diffusion model [16] learns to recover the image from the denoising-like process, i.e., *reverse generation process*. The reverse generation process takes  $T$  time steps to obtain a sequence of noisy data  $\{x_{T-1}, \dots, x_1\}$  and get the data  $x_0$  at the last step. Specifically, it can be formulated as:

$$p_\theta(x_{t-1}|x_t) = \mathcal{N}(x_{t-1} : \mu_\theta(x_t, t), \Sigma_\theta(x_t, t)) \quad (3)$$

The *forward diffusion process* is where we iteratively add Gaussian noise to the data for training the diffusion model to learn  $p_\theta(x_{t-1}|x_t)$ . It is defined as:

$$q(x_t|x_{t-1}) = \mathcal{N}(x_t : \sqrt{\sigma_t}x_{t-1}, (1 - \sigma_t)\mathbf{I}) \quad (4)$$

where  $\sigma$  is the noise schedule.

Nie et al. [24] attempted to find the optimal  $t^*$  where it satisfy that:

$$\begin{aligned} x_{t^*} &= \sqrt{\sigma_{t^*}}x_{\text{adv}} + \sqrt{1 - \sigma_{t^*}}\varepsilon \\ &= \sqrt{\sigma_{t^*}}(x + \delta) + \sqrt{1 - \sigma_{t^*}}\varepsilon \end{aligned} \quad (5)$$

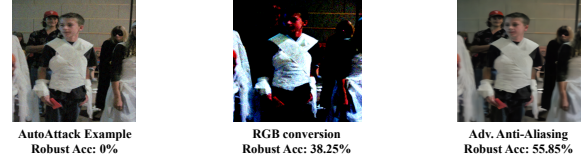


Figure 3. **The vulnerability of adversarial examples to the changes in pixels.** The RGB conversion is performed by converting the images to RGB space after the ImageNet normalization and achieves 38% robust accuracy. The proposed adversarial anti-aliasing is more effective while preserving the image quality.

where  $\varepsilon$  is the Gaussian noise  $\varepsilon \sim \mathcal{N}(0, \mathbf{I})$ . After we obtain the optimal  $t^*$ , we can utilize the reverse generation process over  $x_{\text{adv}}$  to recover the clean  $x$ .

Song et al. [29] utilized the whole reverse generation process with  $T$  time step; they used adversarial sample  $x_{\text{adv}}$  as guidance rather than an intermediate time step state. At each time step  $t$ , the guidance is added to the  $x_t$  after the original reverse generation process and can be formulated as:

$$\nabla_x \log p(x_{\text{adv}}|x_t; t) = -R_t \nabla_{x_t} d(\hat{x}_t, x_{\text{adv}}) \quad (6)$$

where  $R_t$  is the scale factor at  $t$  time step,  $d(\cdot)$  is the distance measurement, and  $\hat{x}_t$  is the estimation for  $x_0$  at  $t$  time step. The  $\hat{x}_t$  is defined as:

$$\hat{x}_t = \frac{x_t - \sqrt{1 - \sigma_t} s_\theta(x_t)}{\sqrt{\sigma_t}} \quad (7)$$

where the  $s_\theta$  known score function is defined as [31].

## 4. Methodology

### 4.1. Motivation

With the advancement of diffusion models, diffusion-based adversarial purification has emerged as a leading approach for adversarial defenses. However, current methods still face significant challenges that impact their effectiveness. Figure 2 illustrates typical diffusion-based purification pipelines from state-of-the-art methods. Nie et al. [24] achieved purification by utilizing the adversarial latent generated by the forward process of adversarial examples. Unfortunately, this approach can introduce adversarial perturbations into the purified examples, as these perturbations persist in the adversarial latent. Song et al. [29] sought to mitigate the impact of adversarial perturbations by using random latents, employing adversarial examples solely as guidance. However, this method requires gradient calculations at each step of the reverse process, making it computationally intensive. Consequently, achieving both **time-efficient** and **perturbation-isolated** diffusion-based adversarial purification remains a challenge. Furthermore, ex-



Figure 4. **The example of proposed adversarial super-resolution.** Our method achieves similar adversarial purification without any gradient calculation of diffusion models.

isting defenses fail to defend against the recently proposed unrestricted adversarial attacks.

## 4.2. Perturbation-Isolated Adversarial Purification

Perturbation-based adversarial examples are precisely calculated based on the gradient of the loss function, whereas unrestricted adversarial examples are sampled near the decision boundary. Despite employing different threat models, both types of attacks produce adversarial examples that are sensitive to pixel changes. Since adversarial examples are designed to be imperceptible compared to clean images, the semantic shapes of objects within the images should correspond to their original labels. Therefore, our defense strategy focuses on extracting the semantic shapes from the adversarial examples and eliminating the adversarial pixel-level details.

### 4.2.1. Adversarial Anti-Aliasing

To achieve effective defenses against both unrestricted and perturbation-based adversarial attacks, it is essential to address their common characteristics. One critical factor is the value range of images: a valid RGB value is an integer between 0 and 255. However, the modifications introduced by various adversarial attacks are often performed using non-integer data types for gradient calculations. These modifications can become ineffective when transformed back to the RGB image format. Figure 3 supports our findings, showing that approximately 38% of adversarial examples from AutoAttack fail with the combinations of RGB conversions and image normalization for deep-learning models. The reasons for this phenomenon could be that adversarial examples are typically located near the decision boundary and are sensitive to pixel changes. However, simple RGB conversion can be effectively compromised by adaptive attacks [1]. Therefore, in this paper, we aim to propose more effective transformations.

Anti-aliasing is a straightforward, zero-shot method for smoothing image details, including adversarial perturbations [21, 32]. Unlike previous works, we have found that anti-aliasing with non-square filters is particularly effective

against adversarial attacks while preserving clean accuracy. Additionally, using the average value from neighboring pixels, excluding the original pixel, has also proven effective. This is because adversarial perturbations are calculated on a pixel-wise basis and are sensitive to pixel changes. These two approaches greatly enhance the effectiveness of anti-aliasing. Even with simple anti-aliasing, we achieve moderate defense performance, underscoring the effectiveness of our approach. The detailed calculation method is discussed in the appendix. Although adversarial anti-aliasing can produce blurred images, the semantic features are preserved because the adversarial perturbation should remain imperceptible. Therefore, it effectively reduces the magnitude of adversarial perturbations while maintaining the semantic information necessary for classification. To maintain the resolution of the output image, we use padding, which is calculated as follows:

$$R_{out} = \lfloor R_{in} + 2 \times \text{Padding} - \text{filter\_size} \rfloor \quad (8)$$

where  $R$  is the shape of the data. We use  $\text{stride} = 1$ .

### 4.2.2. Adversarial Super-Resolution

During the adversarial anti-aliasing phase, we significantly reduce adversarial perturbations by directly decreasing pixel-wise modifications of adversarial examples. However, this approach may not be effective against unrestricted adversarial examples, as they are not generated by adding explicit perturbations. Additionally, blurring the images can negatively impact the clean accuracy of the target model. Super-resolution offers an effective way to recover high-quality images from our adversarial anti-aliased images. Previous super-resolution methods [12, 19] typically modify the original pixels of the low-resolution image and use the residual features of the original low-resolution image. These methods can inadvertently transfer negative effects from the adversarial examples to the final high-resolution images, making them ineffective for adversarial super-resolution. Diffusion-model-based super-resolution [26, 38] provides a more isolated approach for super-resolution. These models generate high-resolution

Table 1. **The standard and robust accuracy against left: AutoAttack ( $\ell_{\text{inf}} = 8/255$ ), right: PGD-EOT ( $\ell_{\text{inf}} = 8/255$ ) on CIFAR10.**

Method	Target Model	Standard Acc(%)	AutoAttack Acc(%)	PGD-EOT Acc(%)
Wu <i>et al.</i> [35]	WideResNet-28-10	85.36	59.18	62.16
Gowal <i>et al.</i> [13]	WideResNet-28-10	87.33	61.72	64.68
Rebuffi <i>et al.</i> [25]	WideResNet-28-10	87.50	65.24	68.89
Wang <i>et al.</i> [33]	WideResNet-28-10	84.85	71.18	68.36
Nie <i>et al.</i> [24]	WideResNet-28-10	89.23	71.03	46.84
Lee <i>et al.</i> [20]	WideResNet-28-10	90.16	70.47	55.82
Song <i>et al.</i> [29]	WideResNet-28-10	92.10	75.45	68.20
Ours	WideResNet-28-10	<b>92.54 ± 1.66</b>	<b>82.02 ± 1.17</b>	<b>80.86 ± 1.33</b>
Rebuffi <i>et al.</i> [25]	WideResNet-70-16	88.54	64.46	68.23
Gowal <i>et al.</i> [13]	WideResNet-70-16	88.74	66.60	69.48
Nie <i>et al.</i> [24]	WideResNet-70-16	91.04	71.84	51.13
Lee <i>et al.</i> [20]	WideResNet-70-16	90.43	66.06	56.88
Song <i>et al.</i> [29]	WideResNet-70-16	93.25	76.60	69.55
Ours	WideResNet-70-16	<b>93.42 ± 1.51</b>	<b>83.65 ± 2.90</b>	<b>81.60 ± 1.75</b>

images through a denoising-like process over randomly sampled noise, using the low-resolution image as conditions.

In this work, we adopt the ResShift method by Yue et al. [38] for our super-resolution process. This super-resolution model can also incorporate benign priors for defense, as it is trained with the clean dataset of the target model. Figure 4 demonstrates that the proposed super-resolution method achieves results comparable to diffusion-based adversarial purification [29], which do not require the calculation of gradient.

### 4.2.3. Adversarial Purification

The proposed adversarial purification is performed by the combination of adversarial anti-aliasing and adversarial super-resolution. We resize the purified images after the adversarial super-resolution for the target model. Additionally, our approach does not require any training of the target model or the defense model.

$$y = \{f(\text{SR}(\text{AA}(x_{\text{adv}})))\} \quad (9)$$

### 4.3. Discussions on Improved Time Efficiency

As previously discussed, employing the entire reverse process with adversarial example guidance is computationally intensive, while using only a partial reverse process diminishes defense performance. In this paper, we propose a two-fold solution to address this issue. First, we introduce an **effective preprocessing approach, specifically anti-aliasing, to mitigate the impact of adversarial perturbations**. Previous research has shown that diffusion-based adversarial purification should avoid introducing adversarial perturbations into the diffusion model. Therefore, a more effective strategy is to remove some of these perturbations

before feeding adversarial examples into the diffusion models. Unlike previous methods that directly utilize adversarial examples for purification, our approach offers a preliminary filtering step.

Second, we employ **diffusion-based super-resolution instead of diffusion-based image generation**. It is well-known that the reverse process of diffusion models is time-consuming, as illustrated in Figure 2, and the gradient calculation exacerbates this issue. However, we may not require the entire reverse process for purification, given that we already have a reference adversarial example, which is also discussed in Nie et al. [24]’s work. Since adversarial perturbations are pixel-wise, we opt for a relatively lightweight generation task, namely super-resolution, which also focuses on pixel modification. The diffusion-based super-resolution method used in this paper requires only tens of steps, compared to the hundreds or thousands of diffusion steps needed in previous works. With these two approaches, we significantly enhance the time efficiency of diffusion-based adversarial purification without compromising defense performance.

## 5. Experiments

### 5.1. Experimental Setup

**Dataset and target models.** We consider CIFAR-10 [18] and ImageNet [10] for major evaluation. For target models, we adopt WideResNet-28-10 and WideResNet-70-16 [39] for CIFAR-10 dataset and ResNet50 [14] for ImageNet dataset. These are commonly adopted backbones for adversarial robustness evaluation.

**Comparisons.** We compared our defense methods with various state-of-the-art defenses by the standardized benchmark: RobustBench [8]. We compare four diffusion-based

adversarial purification methods: Nie et al.’s DiffPure [24], Wang et al.’s [33], Lee et al.’s [20] and Song et al.’s MimicDiffusion [29]. We mainly compare our method with MimicDiffusion as it is the current state-of-the-art method. We use the Score SDE [31] implementation of MimicDiffusion on CIFAR-10 for fair comparisons. The defense methods that use extra data are not compared for fairness. We only evaluate the adversarial purification methods against unrestricted adversarial attacks as the adversarial training’s different threat model.

**Attack settings.** We evaluate our method with both perturbation-based attacks and diffusion-based unrestricted adversarial attacks. For perturbation-based attacks, we select AutoAttack [7], PGD [23]. For diffusion-based unrestricted adversarial attacks, we use DiffAttack [4] and AdvDiff [9] for comparisons. DiffAttack is only evaluated on the ImageNet dataset according to the original paper. To ensure a fair comparison with previous diffusion-based adversarial purification, we include the evaluation against the adaptive attack, i.e., reverse pass differentiable approximation (BPDA) [15]. We also evaluate the performance against PGD+EOT that is discussed in [20]. On CIFAR-10, the attack settings follow DiffPure [24]. On ImageNet, we randomly sample 5 images from each class and average over 10 runs. The PGD+EOT settings all follow Lee et al. [20].

**Implementation details.** We adopt the mean filter with  $[[1, 1], [1, 1]]$  for adversarial anti-aliasing on CIFAR-10, and  $[[1, 1, 1, 1, 1], [1, 1, 0, 1, 1], [1, 1, 1, 1, 1]]$  in ImageNet. ResShift [38] is utilized for adversarial super-resolution. We use the official Score SDE [31] checkpoint for CIFAR-10 and LDM [26] checkpoint for ImageNet to generate UAs. More details and experiment results are given in the appendix.

**Evaluation metrics.** Following Nie et al. [24], we use *standard accuracy* and *robust accuracy* as the evaluation metrics. Both are calculated according to the top-1 classification accuracy.

## 5.2. Attack Performance

### 5.2.1. CIFAR10

**Perturbation-based adversarial attack.** Table 1 presents the defense performance against AutoAttack ( $\ell_{\text{inf}} = 8/255$ ) on the CIFAR10 dataset. The results demonstrate that our proposed method achieves better standard accuracy and robust accuracy than previous attack methods. Because images in the CIFAR10 dataset are only with  $32 \times 32$  resolution, we set our anti-aliasing filter to a relatively small size. Table 2 indicates that the robustness performance of the proposed method is on par with the state-of-the-art method [24]. This finding suggests that our method is more suitable for high-resolution images, as  $32 \times 32$  may not be large enough to effectively extract the semantic shape for our approach. However, we can further enhance our perfor-

Table 2. **The standard and robust accuracy against BPDA ( $\ell_{\text{inf}} = 8/255$ ) on the CIFAR10 dataset with WideResNet-28-10 as the target model.**

Method	Purification	Standard Acc(%)	Robust Acc(%)
Nie et al. [24]( $t^* = 0.0075$ )	Diffusion	91.38	77.62
Nie et al. [24]( $t^* = 0.1$ )	Diffusion	89.23	<b>81.56</b>
Wang et al. [33]	Diffusion	90.36	77.31
Song et al. [29]	Diffusion	91.41	76.45
Ours	Diffusion	<b>91.52 ± 1.28</b>	81.24 ± 2.51

Table 3. **The standard and robust accuracy against AdvDiff on the CIFAR10 dataset.**

Method	Target Model	Standard Acc(%)	Robust Acc(%)
Nie et al. [24]	WideResNet-28-10	95.42	21.56
Wang et al. [33]	WideResNet-28-10	95.86	26.68
Lee et al. [20]	WideResNet-28-10	95.29	24.94
Song et al. [29]	WideResNet-28-10	96.21	23.23
Ours	WideResNet-28-10	<b>96.80 ± 0.37</b>	<b>33.97 ± 0.77</b>

mance by incorporating adversarial purification techniques from previous work.

Our defense’s performance against PGD-EOT showcases its ability to defend against adaptive attacks. This is because our approach focuses on extracting and recovering the semantic features from adversarial images, rather than inferring and denoising the adversarial perturbations. As a result, our defense maintains similar effectiveness against both adaptive and standard attacks.

**Unrestricted adversarial attack.** Unrestricted adversarial examples on the CIFAR10 dataset are challenging to defend against, as shown in Table 3. Our purification method outperforms the previous adversarial purification approach [29] by an average of 10%, validating the effectiveness of our proposed defense.

### 5.2.2. ImageNet

**Perturbation-based adversarial attack.** Tables 4 and 5 demonstrate that the proposed defense method achieves significantly higher performance in both standard accuracy and robust accuracy. Our defense’s standard accuracy notably surpasses previous work, further validating that adversarial super-resolution effectively leverages prior knowledge from the training dataset to achieve better classification accuracy. Adversarial anti-aliasing proves to be particularly effective on the ImageNet dataset, where the filter successfully blurs adversarial perturbations in the detailed pixels of adversarial examples. The performance against PGD-EOT further validates the effectiveness of our proposed defense pipeline.

**Unrestricted adversarial attack.** We present the defense performance of various methods against the unrestricted adversarial attack AdvDiff and DiffAttack in Table 6 and

Table 4. **The standard and robust accuracy against AutoAttack ( $\ell_{\text{inf}} = 8/255$ ) on the ImageNet dataset.**

Method	Target Model	Standard Acc(%)	Robust Acc(%)
Engstrom <i>et al.</i> [8]	ResNet50	62.56	31.06
Wong <i>et al.</i> [34]	ResNet50	55.62	26.95
Salman <i>et al.</i> [27]	ResNet50	64.02	37.89
Bai <i>et al.</i> [2]	ResNet50	67.38	35.51
Nie <i>et al.</i> [24]	ResNet50	68.22	43.89
Song <i>et al.</i> [29]	ResNet50	66.92	61.53
Ours	ResNet50	<b>75.28 ± 1.06</b>	<b>67.61 ± 1.95</b>

Table 5. **The standard and robust accuracy against left: PGD ( $\ell_{\text{inf}} = 4/255$ ), right: PGD+EOT ( $\ell_{\text{inf}} = 4/255$ ) on ImageNet dataset.**

Method	Target Model	Standard Acc(%)	PGD Acc(%)	PGD+EOT Acc(%)
Wong <i>et al.</i> [34]	ResNet50	55.62	26.24	30.51
Salman <i>et al.</i> [27]	ResNet50	64.02	34.96	38.62
Bai <i>et al.</i> [2]	ResNet50	67.38	40.27	43.42
Nie <i>et al.</i> [24]	ResNet50	68.22	42.88	38.71
Lee <i>et al.</i> [20]	ResNet50	70.74	46.31	42.15
Wang <i>et al.</i> [33]	ResNet50	70.17	68.78	40.22
Song <i>et al.</i> [29]	ResNet50	66.92	62.16	52.66
Ours	ResNet50	<b>75.28 ± 1.06</b>	<b>69.75 ± 2.61</b>	<b>66.87 ± 1.85</b>

7. The results indicate that current defenses are ineffective against the recently proposed unrestricted adversarial attacks. The high standard accuracy can be attributed to the strong generative performance of benign diffusion models. Our defense method is capable of achieving significantly higher robust accuracy compared to previous defenses while preserving the standard accuracy.

Table 6. **The standard and robust accuracy against AdvDiff on the ImageNet dataset.**

Method	Target Model	Standard Acc(%)	Robust Acc(%)
Nie <i>et al.</i> [24]	ResNet50	91.48	24.82
Wang <i>et al.</i> [33]	ResNet50	92.31	26.74
Lee <i>et al.</i> [20]	ResNet50	91.80	25.34
Song <i>et al.</i> [29]	ResNet50	92.54	25.35
Ours	ResNet50	<b>97.83 ± 1.36</b>	<b>42.21 ± 3.41</b>

### 5.3. Time efficiency

We evaluate the average time for defending against one adversarial example as shown in Table 8. The results indicate that our proposed method achieves better robust accuracy with significantly lower time costs, as it does not require any gradient calculations over the diffusion model. Notably, our adversarial anti-aliasing can defend against approximately 57% of adversarial examples in just  $3e^{-3}$  seconds. Furthermore, we can enhance the defense performance of our

Table 7. **The standard and robust accuracy against DiffAttack on the ImageNet dataset.**

Method	Target Model	Standard Acc(%)	Robust Acc(%)
Nie <i>et al.</i> [24]	ResNet50	68.22	59.15
Wang <i>et al.</i> [33]	ResNet50	69.54	62.33
Lee <i>et al.</i> [20]	ResNet50	70.74	61.56
Song <i>et al.</i> [29]	ResNet50	66.92	60.17
Ours	ResNet50	<b>75.28 ± 1.06</b>	<b>65.51 ± 1.33</b>

method by combining it with previous purification methods, with only a minimal tradeoff in time cost.

### 5.4. Ablation Study

We perform ablation studies to validate the performance of the proposed methods. We evaluate the defense method against AutoAttack ( $\ell_{\text{inf}} = 8/255$ ) on the ImageNet dataset by default.

**Adversarial Anti-Aliasing.** Despite the satisfactory robustness performance of the proposed adversarial anti-aliasing, the choice of filter settings is critical for optimal defense performance. We present the defense performance with different filters in Figure 5. The results indicate a tradeoff between robust accuracy and standard accuracy. Robust accuracy tends to stabilize when using a filter larger than  $3 \times 3$  in size. Therefore, it is relatively straightforward to identify a suitable filter with a few attempts. Fur-

Table 8. The average time cost of defending one image against PGD ( $\ell_{\text{inf}} = 4/255$ ) on the ImageNet dataset.

Method	Defend Method	Time Cost(s)	Robust Acc(%)
Nie <i>et al.</i> [24]	Diffusion	13.3	42.88
Wang <i>et al.</i> [33]	Diffusion	62.8	68.78
Lee <i>et al.</i> [20]	Diffusion	32.4	46.31
Song <i>et al.</i> [29]	Diffusion	146.1	62.16
Ours	Adversarial Anti-Aliasing	$3e^{-3}$	57.61
+	Adversarial Super-Resolution	<b>1.1</b>	<b>69.75</b>

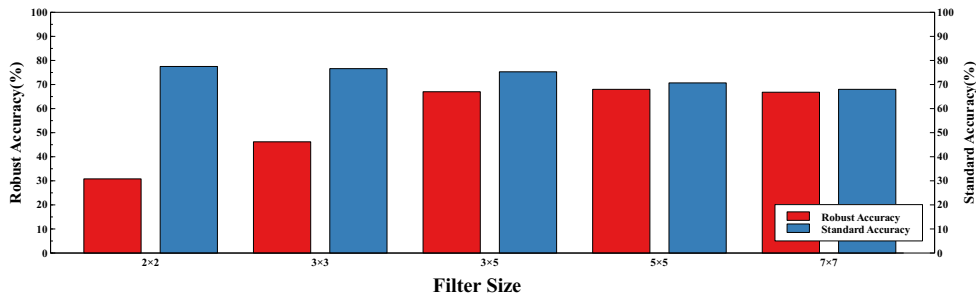


Figure 5. The ablation study of filter size. The weight of the filter at each position is set to 1 except for the center, which we set to 0.

thermore, the filter settings are generalized across different adversarial attacks within the same dataset, as demonstrated in Tables 4, 5, and 6.

Table 9. The ablation study of proposed methods.

(a) The ablation study of proposed adversarial super-resolution.		(b) The performance of integrating our method with previous adversarial purification.	
Method	Robust Acc(%)	Method	Robust Acc(%)
Nie <i>et al.</i> [24]	43.89	Nie <i>et al.</i> [24]	43.89
Song <i>et al.</i> [29]	61.53	+ Ours	69.44
Adversarial AA	55.85	Song <i>et al.</i> [29]	61.53
Adversarial SR	41.23	+ Ours	72.18
Adversarial AA+SR	<b>67.61</b>		

**Adversarial Super-Resolution.** The proposed adversarial super-resolution achieves a similar purification function to previous diffusion-based adversarial purification methods, but without the need for computationally expensive gradient calculations. Table 9a demonstrates that our method slightly outperforms traditional adversarial purification when using anti-aliased adversarial examples as input. However, it is crucial to use anti-aliased adversarial examples for optimal performance in adversarial super-resolution, as we do not account for the adversarial gradient during the super-resolution process.

**Adversarial Purification.** We can enhance diffusion-based adversarial purification methods from previous works by replacing the adversarial input with the adversarial examples

after the proposed purification. The processed adversarial examples are more benign and closer to the clean images, thereby enabling better purification performance, as demonstrated in Table 9b.

## 6. Conclusion

In this paper, we present an effective and efficient adversarial defense method against both perturbation-based and unrestricted adversarial attacks. The proposed techniques, adversarial anti-aliasing and adversarial super-resolution, effectively eliminate adversarial modifications and recover benign images with minimal computational overhead. Comprehensive experiments on the CIFAR-10 and ImageNet datasets validate that our proposed defense outperforms state-of-the-art defense methods. Our work demonstrates that simple adversarial anti-aliasing can achieve moderate model robustness with almost no additional cost. Furthermore, the proposed super-resolution method can perform adversarial purification without requiring the calculation of the diffusion model’s gradient. We hope our work will serve as a baseline for the further development of adversarial defenses.

## References

- [1] Anish Athalye, Nicholas Carlini, and David Wagner. Obfuscated gradients give a false sense of security: Circumventing defenses to adversarial examples. In *International conference on machine learning*, pages 274–283. PMLR, 2018. 4

- [2] Tao Bai, Jinqi Luo, Jun Zhao, Bihan Wen, and Qian Wang. Recent advances in adversarial training for adversarial robustness. In *Proceedings of the Thirtieth International Joint Conference on Artificial Intelligence*, pages 4312–4321, 2021. 7
- [3] Nicholas Carlini and David Wagner. Towards evaluating the robustness of neural networks. In *2017 IEEE Symposium on Security and Privacy (SP)*, pages 39–57. IEEE, 2017. 1
- [4] Jianqi Chen, Hao Chen, Keyan Chen, Yilan Zhang, Zhengxia Zou, and Zhenwei Shi. Diffusion models for imperceptible and transferable adversarial attack. *arXiv preprint arXiv:2305.08192*, 2023. 6
- [5] Xinquan Chen, Xitong Gao, Juanjuan Zhao, Kejiang Ye, and Cheng-Zhong Xu. Advdiffuser: Natural adversarial example synthesis with diffusion models. In *Proceedings of the IEEE/CVF International Conference on Computer Vision*, pages 4562–4572, 2023. 1
- [6] Zhaoyu Chen, Bo Li, Shuang Wu, Kaixun Jiang, Shouhong Ding, and Wenqiang Zhang. Content-based unrestricted adversarial attack. *arXiv preprint arXiv:2305.10665*, 2023. 1
- [7] Francesco Croce and Matthias Hein. Reliable evaluation of adversarial robustness with an ensemble of diverse parameter-free attacks. In *International conference on machine learning*, pages 2206–2216. PMLR, 2020. 6
- [8] Francesco Croce, Maksym Andriushchenko, Vikash Sehwag, Edoardo DeBenedetti, Nicolas Flammarion, Mung Chiang, Prateek Mittal, and Matthias Hein. Robustbench: a standardized adversarial robustness benchmark. In *Thirty-fifth Conference on Neural Information Processing Systems Datasets and Benchmarks Track*, 2021. 5, 7
- [9] Xuelong Dai, Kaisheng Liang, and Bin Xiao. Advdiff: Generating unrestricted adversarial examples using diffusion models. *arXiv preprint arXiv:2307.12499*, 2023. 1, 6
- [10] Jia Deng, Wei Dong, Richard Socher, Li-Jia Li, Kai Li, and Li Fei-Fei. Imagenet: A large-scale hierarchical image database. In *2009 IEEE conference on computer vision and pattern recognition*, pages 248–255. Ieee, 2009. 5
- [11] Prafulla Dhariwal and Alexander Nichol. Diffusion models beat gans on image synthesis. *Advances in Neural Information Processing Systems*, 34:8780–8794, 2021. 1
- [12] Shangqi Gao and Xiahai Zhuang. Multi-scale deep neural networks for real image super-resolution. In *Proceedings of the IEEE/CVF conference on computer vision and pattern recognition workshops*, pages 0–0, 2019. 4
- [13] Sven Gowal, Sylvestre-Alvise Rebuffi, Olivia Wiles, Florian Stimpberg, Dan Andrei Calian, and Timothy A Mann. Improving robustness using generated data. *Advances in Neural Information Processing Systems*, 34:4218–4233, 2021. 1, 2, 5
- [14] Kaiming He, Xiangyu Zhang, Shaoqing Ren, and Jian Sun. Deep residual learning for image recognition. In *Proceedings of the IEEE conference on computer vision and pattern recognition*, pages 770–778, 2016. 1, 5
- [15] Mitch Hill, Jonathan Craig Mitchell, and Song-Chun Zhu. Stochastic security: Adversarial defense using long-run dynamics of energy-based models. In *International Conference on Learning Representations*, 2021. 6
- [16] Jonathan Ho, Ajay Jain, and Pieter Abbeel. Denoising diffusion probabilistic models. *Advances in Neural Information Processing Systems*, 33:6840–6851, 2020. 3
- [17] Gaojie Jin, Xinpeng Yi, Dengyu Wu, Ronghui Mu, and Xiaowei Huang. Randomized adversarial training via Taylor expansion. In *Proceedings of the IEEE/CVF Conference on Computer Vision and Pattern Recognition*, pages 16447–16457, 2023. 2
- [18] Alex Krizhevsky, Geoffrey Hinton, et al. Learning multiple layers of features from tiny images. 2009. 5
- [19] Christian Ledig, Lucas Theis, Ferenc Huszar, Jose Caballero, Andrew Cunningham, Alejandro Acosta, Andrew Aitken, Alykhan Tejani, Johannes Totz, Zehan Wang, et al. Photo-realistic single image super-resolution using a generative adversarial network. In *Proceedings of the IEEE conference on computer vision and pattern recognition*, pages 4681–4690, 2017. 4
- [20] Minjong Lee and Dongwoo Kim. Robust evaluation of diffusion-based adversarial purification. In *Proceedings of the IEEE/CVF International Conference on Computer Vision*, pages 134–144, 2023. 2, 5, 6, 7, 8
- [21] Bin Liang, Hongcheng Li, Miaoqiang Su, Xirong Li, Wenchang Shi, and Xiaofeng Wang. Detecting adversarial image examples in deep neural networks with adaptive noise reduction. *IEEE Transactions on Dependable and Secure Computing*, 18(1):72–85, 2018. 4
- [22] Ze Liu, Yutong Lin, Yue Cao, Han Hu, Yixuan Wei, Zheng Zhang, Stephen Lin, and Baining Guo. Swin transformer: Hierarchical vision transformer using shifted windows. In *Proceedings of the IEEE/CVF international conference on computer vision*, pages 10012–10022, 2021. 1
- [23] Aleksander Madry, Aleksandar Makelov, Ludwig Schmidt, Dimitris Tsipras, and Adrian Vladu. Towards deep learning models resistant to adversarial attacks. In *International Conference on Learning Representations*, 2018. 1, 2, 6
- [24] Weili Nie, Brandon Guo, Yujia Huang, Chaowei Xiao, Arash Vahdat, and Anima Anandkumar. Diffusion models for adversarial purification. In *International Conference on Machine Learning (ICML)*, 2022. 1, 2, 3, 5, 6, 7, 8
- [25] Sylvestre-Alvise Rebuffi, Sven Gowal, Dan Andrei Calian, Florian Stimpberg, Olivia Wiles, and Timothy A Mann. Data augmentation can improve robustness. *Advances in Neural Information Processing Systems*, 34:29935–29948, 2021. 2, 5
- [26] Robin Rombach, Andreas Blattmann, Dominik Lorenz, Patrick Esser, and Björn Ommer. High-resolution image synthesis with latent diffusion models. In *Proceedings of the IEEE/CVF Conference on Computer Vision and Pattern Recognition*, pages 10684–10695, 2022. 1, 4, 6
- [27] Hadi Salman, Andrew Ilyas, Logan Engstrom, Ashish Kapoor, and Aleksander Madry. Do adversarially robust imagenet models transfer better? In *Proceedings of the Advances in Neural Information Processing Systems*, 2020. 7
- [28] Pouya Samangouei, Maya Kabkab, and Rama Chellappa. Defense-gan: Protecting classifiers against adversarial attacks using generative models. In *International Conference on Learning Representations*, 2018. 2

- [29] Kaiyu Song, Hanjiang Lai, Yan Pan, and Jian Yin. Mimicdiffusion: Purifying adversarial perturbation via mimicking clean diffusion model. In *Proceedings of the IEEE/CVF Conference on Computer Vision and Pattern Recognition*, pages 24665–24674, 2024. [1](#), [2](#), [3](#), [5](#), [6](#), [7](#), [8](#)
- [30] Yang Song, Rui Shu, Nate Kushman, and Stefano Ermon. Constructing unrestricted adversarial examples with generative models. In *Proceedings of the Advances in Neural Information Processing Systems*, pages 8322–8333, 2018. [3](#)
- [31] Yang Song, Jascha Sohl-Dickstein, Diederik P Kingma, Abhishek Kumar, Stefano Ermon, and Ben Poole. Score-based generative modeling through stochastic differential equations. In *International Conference on Learning Representations*, 2021. [2](#), [3](#), [6](#)
- [32] Cristina Vasconcelos, Hugo Larochelle, Vincent Dumoulin, Rob Romijnders, Nicolas Le Roux, and Ross Goroshin. Impact of aliasing on generalization in deep convolutional networks. In *Proceedings of the IEEE/CVF International Conference on Computer Vision*, pages 10529–10538, 2021. [4](#)
- [33] Jinyi Wang, Zhaoyang Lyu, Dahua Lin, Bo Dai, and Hongfei Fu. Guided diffusion model for adversarial purification. *arXiv preprint arXiv:2205.14969*, 2022. [2](#), [5](#), [6](#), [7](#), [8](#)
- [34] Eric Wong, Leslie Rice, and J. Zico Kolter. Fast is better than free: Revisiting adversarial training. In *Proceedings of the International Conference on Learning Representations*, 2020. [7](#)
- [35] Dongxian Wu, Shu-Tao Xia, and Yisen Wang. Adversarial weight perturbation helps robust generalization. *Advances in neural information processing systems*, 33:2958–2969, 2020. [2](#), [5](#)
- [36] Tiange Xiang, Chaoyi Zhang, Yang Song, Jianhui Yu, and Weidong Cai. Walk in the cloud: Learning curves for point clouds shape analysis. In *Proceedings of the IEEE/CVF International Conference on Computer Vision (ICCV)*, pages 915–924, 2021. [1](#)
- [37] Jongmin Yoon, Sung Ju Hwang, and Juho Lee. Adversarial purification with score-based generative models. In *International Conference on Machine Learning*, pages 12062–12072. PMLR, 2021. [2](#)
- [38] Zongsheng Yue, Jianyi Wang, and Chen Change Loy. Resshift: Efficient diffusion model for image super-resolution by residual shifting. *Advances in Neural Information Processing Systems*, 36, 2024. [4](#), [5](#), [6](#)
- [39] Sergey Zagoruyko and Nikos Komodakis. Wide residual networks. *arXiv preprint arXiv:1605.07146*, 2016. [5](#)

# Supplementary Materials for Gradient-Free Adversaria Purification with Diffusion Models

Anonymous CVPR submission

Paper ID 5371

## A. Details for Adversarial Anti-Aliasing

We give the details on the implementation of proposed adversarial anti-aliasing in Figure 1. We use 1D convolution on each RGB channel of the adversarial image and clip the additional dimensions according to the input resolution. After that, we convert the anti-aliased image tensor to the RGB image for adversarial super-resolution.

The proposed adversarial anti-aliasing utilizes the mean value from a pixel’s neighborhood and can be seen as a direct method for reducing adversarial perturbations. It is well-known in image classification that the areas contributing most to classification results are typically located at the center of the main object, where they are rich in textures. Consequently, the anti-aliasing filter can effectively neutralize adversarial perturbations in these regions, which often exhibit significant changes in RGB values and gradients of the classification loss function [? ], especially in high-resolution images. By applying blurring, the proposed adversarial anti-aliasing method can significantly decrease the magnitude of adversarial perturbations. The worst case of the proposed method occurs in simple backgrounds, such as the sky. However, these areas generally have minimal impact on the final classification results.

## B. Details for Adversarial Super-Resolution

Adversarial super-resolution focuses on recovering details from low-quality inputs. We employ ResShift, trained on the ImageNet dataset, and evaluate its performance on both the ImageNet and CIFAR-10 datasets. For CIFAR-10, the performance of ResShift is slightly reduced due to the dataset’s low resolution. An ablation study exploring different settings for adversarial super-resolution is presented in Table 1. The results indicate that using ResShift with a  $256 \times 256$  resolution input yields the best performance. Our work also supports the adoption of other super-resolution diffusion models. However, for improved robust accuracy, it is advisable to use our purified images as input for diffusion-based purification rather than replacing the super-resolution model.

Table 1. The ablation study on adversarial super-resoultion against AutoAttack ( $\ell_{inf} = 8/255$ ) on the ImageNet dataset.

Method	Robust Accuracy(%)	Time(s)
ResShift $256 \times 256$	67.61	1.1
ResShift $64 \times 64$	55.98	$1e^{-1}$
LDM $128 \times 128$	61.35	9.0

## C. Detail Experiment Settings

Our experiment is implemented with PyTorch on two NVIDIA GeForce RTX 3090 GPUs. For the CIFAR10 dataset, we upscale the adversarial anti-aliased images with PyToch to  $64 \times 64$  resolution for ResShift. We use ResShift default v3 parameter for our experiments.

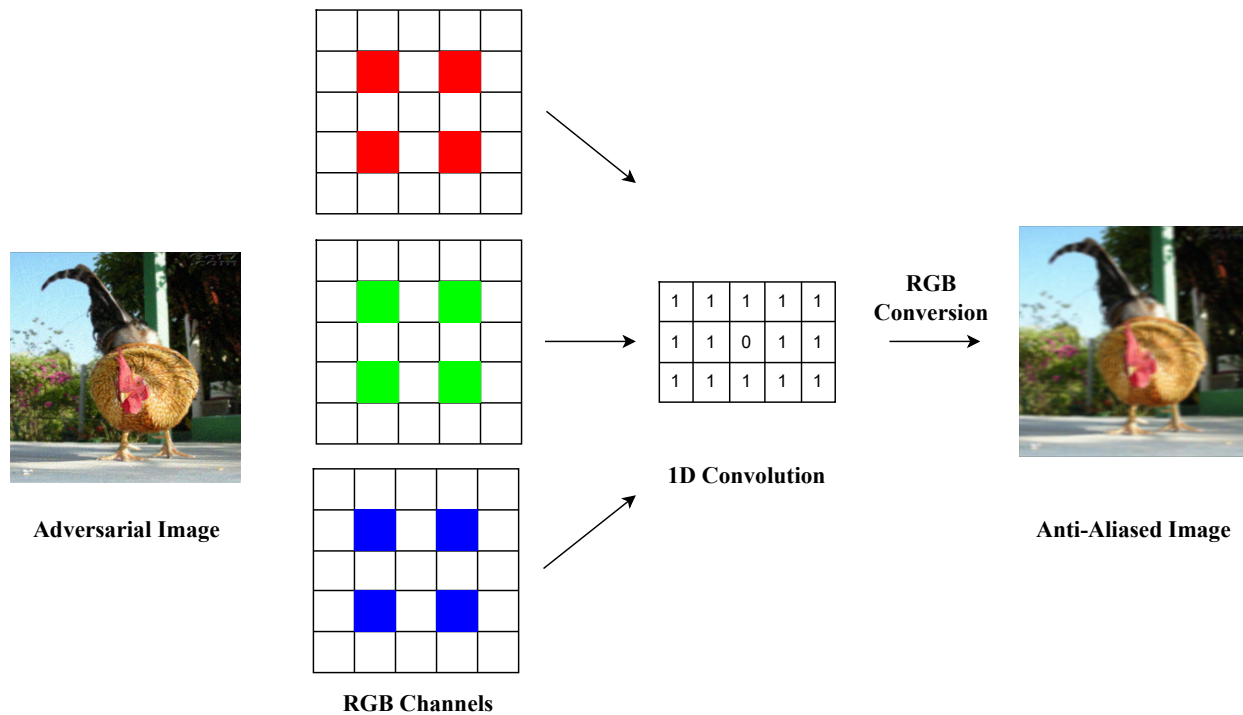


Figure 1. **The adversarial anti-aliasing pipeline.** We use 1D convolution on each RGB channel of the input adversarial image for adversarial anti-aliasing. After that, we convert the output RGB channels to the output image.

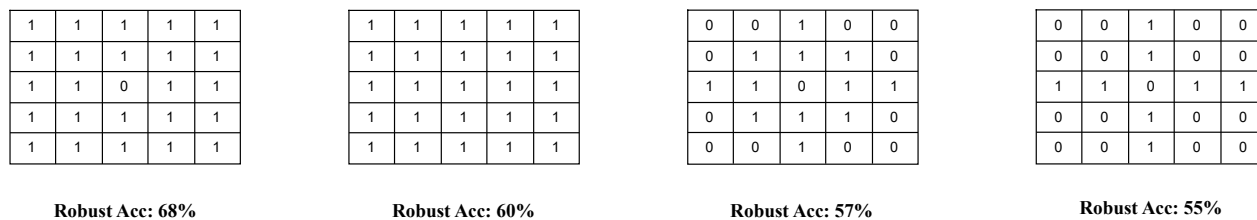


Figure 2. **The defense performance of various filter weights against AutoAttack ( $\ell_{\text{inf}} = 8/255$ ) on the ImageNet dataset.** We use 1 for better understanding, while we set to the mean value according to the number of 1 blocks in the experiments.

## 028 D. Additional Experiments

029 We further report additional experiments against various adversaries on CIFAR10, as shown in Table 2 and 3. We also  
 030 perform adversarial attacks on the eyeglasses attribute of the high-resolution CelebA-HQ dataset following Nie et al. [?]’s  
 031 experiment settings on Table 4. The results demonstrate that our proposed defense outperforms state-of-the-art diffusion-  
 032 based adversarial purification.

## 033 E. Filter Selection

034 We discuss the choice of filter settings in the ablation study. However, it is also critical to design the filter weight for  
 035 the adversarial anti-aliasing. Figure 2 demonstrates that the selection of filter weight is empirical and achieves the best  
 036 performance on setting the mean value except for the center.

Table 2. The defense performance against AutoAttack ( $\ell_2 = 0.5$ ) on the CIFAR10 dataset.

Method	Target Model	Standard Accuracy(%)	Robust Accuracy(%)
Rony <i>et al.</i> [? ]	WideResNet-28-10	89.05	66.41
Ding <i>et al.</i> [? ]	WideResNet-28-10	88.02	67.77
Rebuffi <i>et al.</i> [? ]	WideResNet-28-10	91.79	78.32
Wang <i>et al.</i> [? ]	WideResNet-28-10	92.00	75.28
Nie <i>et al.</i> [? ]	WideResNet-28-10	91.38	78.98
Song <i>et al.</i> [? ]	WideResNet-28-10	<b>92.84</b>	81.52
Ours	WideResNet-28-10	$92.54 \pm 1.66$	<b><math>84.90 \pm 2.82</math></b>
Gowal <i>et al.</i> [? ]	WideResNet-70-16	90.90	74.03
Rebuffi <i>et al.</i> [? ]	WideResNet-70-16	92.41	80.86
Nie <i>et al.</i> [? ]	WideResNet-70-16	93.24	81.17
Song <i>et al.</i> [? ]	WideResNet-70-16	92.51	83.60
Ours	WideResNet-70-16	<b><math>93.42 \pm 1.51</math></b>	<b><math>87.60 \pm 2.35</math></b>

Table 3. The defense performance against C&W ( $\ell_2 = 8/255$ , EOT=50) on the CIFAR10 dataset.

Method	Target Model	Standard Accuracy(%)	Robust Accuracy(%)
Wang <i>et al.</i> [? ]	WideResNet-28-10	21.30	21.71
Nie <i>et al.</i> [? ]	WideResNet-28-10	<b>93.53</b>	47.65
Song <i>et al.</i> [? ]	WideResNet-28-10	90.34	89.91
Ours	WideResNet-28-10	$92.54 \pm 1.66$	<b><math>92.61 \pm 4.52</math></b>

Table 4. The defense performance against BDPA+EOT ( $\ell_{\text{inf}} = 16/255$ ) on the CelebA-HQ dataset.

Method	Defend Method	Standard Accuracy(%)	Robust Accuracy(%)
Richardson <i>et al.</i> [? ]	GAN	93.95	75.00
Nie <i>et al.</i> [? ]	Diffusion	93.77	90.63
Song <i>et al.</i> [? ]	Diffusion	94.52	93.81
Ours	Diffusion	<b><math>98.89 \pm 0.55</math></b>	<b><math>95.92 \pm 2.68</math></b>

## F. Limitation

Despite achieving significantly higher time efficiency and better defense performance than previous diffusion-based adversarial purification methods, our defense approach still has several limitations. One drawback is that the quality of adversarial examples after purification can be relatively low compared to previous purification methods. Therefore, we recommend using the purified images primarily for detecting adversarial inputs. Another limitation is that the robust accuracy against universal adversarial examples (UAEs) is still not on par with perturbation-based adversarial attacks. We aim to address and improve these limitations in future work.

037

038

039

040

041

042

043